Wear 290–291 (2012) 74–85

Contents lists available at SciVerse ScienceDirect

Wear

journal homepage: www.elsevier.com/locate/wear

Reciprocal dry sliding wear behaviour of B_4C_p reinforced aluminium alloy matrix composites

F. Toptan [a,b,*], I. Kerti [a], L.A. Rocha [b,c]

[a] Yildiz Technical University, Department of Metallurgical and Materials Engineering, Faculty of Chemistry & Metallurgy, Davutpasa Campus, 34210 Esenler, Istanbul, Turkey
[b] Centre for Mechanics and Materials Technologies (CT2M), Universidade do Minho, Azurém, 4800-058 Guimarães, Portugal
[c] Universidade do Minho, Dept. Eng. Mecânica, Azurém, 4800-058 Guimarães, Portugal

ARTICLE INFO

Article history:
Received 9 September 2011
Received in revised form
22 May 2012
Accepted 23 May 2012
Available online 31 May 2012

Keywords:
Sliding wear
Metal-matrix composite
Electron microscopy
Wear testing

ABSTRACT

In the present work, AlSi9Cu3Mg alloy matrix composites reinforced with 15 and 19 vol% B_4C_p were produced by squeeze casting route at 850 °C under low vacuum. Titanium-containing flux (K_2TiF_6) was used to promote the wetting between B_4C and liquid aluminium metal. It was found, from the microstructural observations, that the wetting improved by the formation of a thin Ti-rich reaction layer. In order to investigate the wear properties, the samples were subjected to reciprocating wear tests against AISI 4140 pin under dry sliding conditions. The effect of B_4C volume fraction, sliding velocity, applied load and sliding distance on reciprocal dry wear behaviour of composites was studied using general full factorial experimental design. The effects of factors and interactions on the coefficient of friction (COF) and the wear rate values of both composite specimens and counter materials were studied. Worn surfaces and wear debris were characterised using field emission gun scanning electron microscope (FEG-SEM), Energy Dispersive X-Ray Spectroscopy (EDS), optical microscope (OM) and X-Ray diffraction (XRD). From microstructural investigations, wear mechanism was suggested as a combination of adhesive, abrasive, and delamination wear.

© 2012 Elsevier B.V. All rights reserved.

1. Introduction

Particulate reinforced aluminium matrix composites (AMCs) are attractive metal matrix composite (MMC) materials due to their strength, ductility and toughness as well as their ability to be processed by conventional methods [1]. AMCs can be reinforced with various oxides, carbides, nitrides and borides [2–7]. While SiC and Al_2O_3 are the most common reinforcing materials in AMCs, limited research has been conducted on B_4C reinforced AMCs due to the higher cost of B_4C powders [8,9]. However, B_4C is an attractive reinforcement material because of its excellent chemical and thermal stability; most importantly, B_4C has lower density and higher hardness relative to SiC and Al_2O_3 (density values are 2.52, 3.21 and 3.92 g/cm^3 and Knoop Hardness values are 2800, 2480 and 2000, respectively) [8,10–14].

Al–B_4C composites can be processed with low-cost casting routes [3,15–18]. However, in the literature, particle volume fraction values are generally below 15% in cast Al–B_4C composites [15–27]. Relatively higher nominal B_4C volume fractions are used in some works [4,8], however, within these works, there is no information about particle addition yields or actual volume fraction values. It is difficult to obtain high particle addition yields due to the poor wetting between Al and B_4C especially below 1100 °C which makes it difficult to produce Al–B_4C composites by mixing particles into the liquid phase [28]. Apart from wetting, controlling of the interphases occurring at the Al–B_4C interface is also important in the production of cast Al–B_4C composites [29].

It has been reported that the transition metal carbides, borides and nitrides are better wetted than covalently and ionically bonded ceramics [30]. Titanium is one of the reactive metals that can be used to increase wettability in Al–B_4C system [28,31]. Due to the high chemical affinity to boron, titanium easily forms TiC and TiB_2 on the surfaces of boron carbide in Al–B_4C composites and improves wettability as well as particle addition yields. Furthermore, this reaction layer that contains TiC and TiB_2 acts as a "reaction barrier" and limits the undesirable interfacial reactions that can be occurred on the interface. There are some works available in the literature with cast production of Al–B_4C composites with addition of titanium. Kennedy and Brampton produced Al–B_4C composites with addition of K–Al–Ti–F flux [28,32]. However, in these works, volume fraction of B_4C particles is maximum 10%.

Besides wetting and particle addition yield, other common problems in cast-AMCs are difficulties of obtaining homogeneous particle distribution and lowering the porosity. The amount of

* Corresponding author at: Centre for Mechanics and Materials Technologies (CT2M), Universidade do Minho, Azurém, 4800-058 Guimarães, Portugal. Tel.: +351 253 510 220; fax: +351 253 516 007.
E-mail address: ftoptan@dem.uminho.pt (F. Toptan).

0043-1648/$ - see front matter © 2012 Elsevier B.V. All rights reserved.
http://dx.doi.org/10.1016/j.wear.2012.05.007

porosity, and its size and distribution are very important in controlling the material's mechanical properties in a cast MMCs. In vortex casting, the vortex sucks air bubbles in the melt resulting in large amounts of porosities in cast MMCs [33,34]. Laden et al. reported that pores have been created by the vortex during the process and the resulting porosity has been about 5% by volume [35]. On the other hand, increasing particle ratio and decreasing particle size also increase porosity amount in cast MMCs [36,37]. Mazahery and Shabani produced A356 matrix B_4C reinforced (5, 7.5, 10, 12.5, and 15 vol%) composites by squeeze casting route and reported the porosity values as approximately between 0.5% and 2% [26]. In another work, Canakci and Arslan produced AA2024 matrix B_4C reinforced (3, 5, 7, 10 vol%) composites by stir casting route and reported the porosity values as approximately between 2.1% and 3.1% [19].

The dry sliding of AMCs has been widely studied. It is well known that hard ceramic particles improve wear resistance as compared to unreinforced matrix material. The wear rate is related to sliding velocity, particle size, hardness, normal load, chemical composition of the matrix material, particle volume fraction and particle homogeneity [38]. Studies on dry sliding wear in MMCs have been performed with a variety of matrix materials and reinforcements [39]. While SiC and Al_2O_3 reinforced AMCs are the most studied, limited research have been conducted on dry sliding wear of Al–B_4C composites. Generally, pin-on-disc wear test was used in order to study the dry sliding behaviour of Al–B_4C composites [4,20,22,24,25,39,40]. On the other hand, studies on reciprocal dry sliding wear of Al–B_4C composites are very limited and within these studies, contact pressures are relatively high which is higher than the yield strength of matrix alloys [41–43].

Wear behaviour of AMCs is generally investigated by the effect of a single factor, such as sliding distance, sliding speed or contact pressure, on the wear performance. However, the interactions of the factors have certain degree of effects, sometime even strong effects, on the wear behaviour of composites [44]. Several studies are available in the literature on statistical studies of wear behaviour AMCs [44–54], however, there is no study available on reciprocal dry sliding wear of Al–B_4C composites.

In the present work, AlSi9Cu3Mg alloy matrix composites reinforced with 15 and 19 vol% B_4C_p were produced by squeeze casting route at 850 °C under low vacuum. Titanium-containing flux (K_2TiF_6) was used to overcome the wetting problem between B_4C and liquid aluminium metal. The effects of B_4C volume fraction, sliding velocity, applied load and sliding distance on reciprocal dry wear behaviour of composites were studied using a general full factorial experimental design. The effects of factors and interactions on the average COF values and wear rate values both in composite specimens and counter materials were studied. Worn surfaces and wear debris were characterised using SEM, EDS, OM and XRD in order to investigate the wear mechanism.

2. Experimental procedure

2.1. Materials

AlSi9Cu3Mg aluminium alloy was used as a matrix material (Table 1) and B_4C particles with an average particle size 32 μm were used as reinforcement. In order to enhance the wettability of B_4C powders and improve their incorporation behaviour into aluminium melts, potassium fluotitanate (K_2TiF_6) flux was used.

2.2. Composite production

15 and 19 vol% B_4C particulate reinforced AMCs were produced in a boron nitride coated graphite crucible using vacuum controlled induction furnace. Mixture of B_4C particles and the K_2TiF_6 flux (with 0.1 Ti/B_4C ratio) were added into the melt at 850 °C with mechanical stirring which creates vortex at 1000 rpm. Finally, the melt was poured into a metal mould at 900 °C casting temperature and solidified under hydraulic press at 104 MPa. From melting to pouring, the process was conducted under low vacuum atmosphere at 2.5 mbar.

2.3. Characterisation of as-cast composites

Metallographic samples sectioned from the cast bars were prepared using diamond grinders and water based diamond and colloidal silica suspensions up to 0.04 μm grain size. As-cast microstructures were examined under the JEOL JSM 7000F field emission gun scanning electron microscope (FEG-SEM) equipped with an Oxford/Inca EDS. Vickers hardness was measured using an Eseway macrohardness tester at a load of 30 kg f. Volume fraction of particulates was measured by metallographic image analysis technique using the Leica ICM 1000 OM and QWin-V 2.8 image analysis software. In order to measure the volume fractions, an average of 200 measurements were performed in horizontal and perpendicular cross-sections of as-cast composite bars. Experimental volume fraction values are compared with the theoretical volume fraction values and particle addition yield values were calculated.

Density values were measured using the Archimedes principle. Density values were calculated with the following formula:

$$\rho = \frac{A}{A-B}(\rho_0 - d) + d \quad (1)$$

where ρ is the density of the specimen in g/cm^3, A is the weight in the air in g, B is the weight in the liquid in g, ρ_0 is the density of the liquid in g/cm^3 and d is the density of the air in g/cm^3. Experimental density values are compared with the theoretical density values and % porosity values were calculated.

2.4. Wear tests

2.4.1. Design of experiments

2^4 full factorial design method was chosen for the design of reciprocating wear testing experiments. Experiments were planned by varying volume fraction, load, sliding velocity and sliding distance. Two levels of each factor were chosen for the study. Volume fraction levels were 15 and 19%, sliding velocity levels were 0.02 and 0.03 m/s, load levels were 20 and 40 N and sliding distance levels were 200 and 400 m. The levels selected for each factor in the design are shown in Table 2. Minitab 15 statistical software was used for designing the experiments. The plan of experiments was prepared by randomising the experiments in order to avoid the accumulation of errors. The experiments were conducted based on the randomised run order as given in Table 3. Average COF values and wear rate values both

Table 1
Chemical composition of AlSi9Cu3Mg matrix material.

Al	Si	Fe	Mn	Cr	Ni	Cu	Mg	Pb	Sn	Ti	Zn
82.8	10.14	1.29	0.432	0.021	0.032	2.99	1.49	0.372	0.008	0.084	0.616

in composite specimens and counter materials were taken as responses.

2.4.2. Experimental procedure of wear tests

The wear tests were performed using a PLINT TE 67/R tribometer with a reciprocating plate adaptor. Before the wear tests, each specimen polished with the same procedure was used for microstructure investigations. Counter material surfaces were grinded using SiC papers and polished up to 0.04 μm grain size using water based diamond and colloidal silica suspensions. Before starting the wear tests, each specimen was cleaned with propanol in ultrasonic cleaner for 10 min. The tests were performed against a counter material of an AISI 4140 steel pin with 5 mm diameter in laboratory air conditions. The stroke length was chosen as 10 mm for each test.

After each test, composite samples and pins (counter material) were ultrasonically cleaned for 10 min and weight loss values were measured using a sensitive balance with an accuracy of 0.1 mg. The formula used to convert the weight loss into wear rate is

$$W_w = \frac{\Delta W}{s} \quad (2)$$

where W_w is the wear rate in mg/m, ΔW is the weight difference of the sample before and after the test in mg and S is the total sliding distance in m.

Finally, wear tracks were examined under the FEI Nova 200 FEG-SEM equipped with EDAX, Pegasus X4M EDS/EBSD.

Table 2
Factors and their levels chosen for 2^4 full factorial design.

Level	Volume fraction (%)	Sliding velocity (m/s)	Load (N)	Sliding distance (m)
−1	15	0.02	20	200
+1	19	0.03	40	400

Table 3
Plan of experiments.

Std. order	Run order	Factor 1 A: volume fraction (%)	Factor 2 B: velocity (m/s)	Factor 3 C: load (N)	Factor 4 D: distance (m)
2	1	19	0.02	20	200
9	2	15	0.02	20	400
12	3	19	0.03	20	400
7	4	15	0.03	40	200
8	5	19	0.03	40	200
14	6	19	0.02	40	400
16	7	19	0.03	40	400
11	8	15	0.03	20	400
1	9	15	0.02	20	200
13	10	15	0.02	40	400
3	11	15	0.03	20	200
5	12	15	0.02	40	200
6	13	19	0.02	40	200
4	14	19	0.03	20	200
10	15	19	0.02	20	400
15	16	15	0.03	40	400

3. Results and discussion

3.1. Microstructure of as-cast composites

In order to achieve the desired properties in MMC materials, homogeneous particle distribution should be obtained and wettability of reinforcing materials should be optimised [55]. Relatively homogeneous particle distribution was observed on microstructure of composites as shown in Fig. 1.

The potential reactions that could take place in the Al–Ti–B_4C system are reported by Shen et al. Since the reaction which produces TiB_2 and TiC has the lowest Gibbs free energy, ΔG, in the Al–Ti–B_4C system, the most favourable reaction products are TiB_2 and TiC in the process temperatures, which was used in the present work [56]. Fig. 2 shows the SEM images and matching Ti elemental maps for each specimen. As can be seen on the Ti X-ray maps, there are continuous Ti containing layers surrounding B_4C particles which is concluded as consisting of TiB_2 and TiC.

Volume fraction (nominal and experimental), particle addition yield and hardness values are given in Table 4. As can be seen from the table, relatively high volume fraction composites produced with 91.54 and 87.02% particle addition yields for 15% and 19% B_4C reinforced composites, respectively. There is very limited information available on the literature related to particle addition yield values in cast Al–B_4C composites. Due to the low wettability, particle addition yield values are relatively low without any surface modification onto boron carbide particles. Canakci and Arslan produced AA2024 matrix B_4C particle reinforced composites by vortex method and reported that, for composites produced with particles between 49 and 16.5 μm size, particle addition yield is 97% for nominal 3% volume fraction and 65% for nominal 10% fraction [19]. Kennedy and Brampton reported 100% approximate yield in composites produced with stir casting using K–Al–Ti–F flux in order to enhance wettability. However, in the study, nominal particle ratio is just 5 wt% [28].

Density (theoretical and experimental) and porosity values are also given in Table 4. In the present study, due to the applied vacuum during the process, porosity values are fairly low compared to the literature. For instance, Mazahery and Shabani detected approximately 2% porosity in squeeze-cast A356-15 vol%

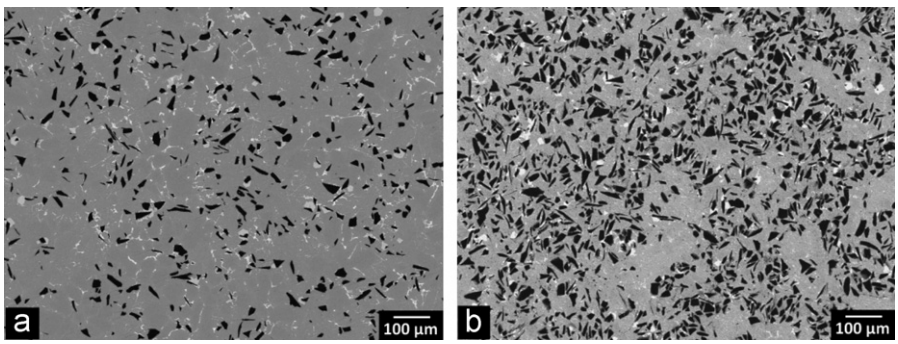


Fig. 1. Back-scattered electron (BSI) SEM images of (a) 15% and (b) 19% reinforced composites.

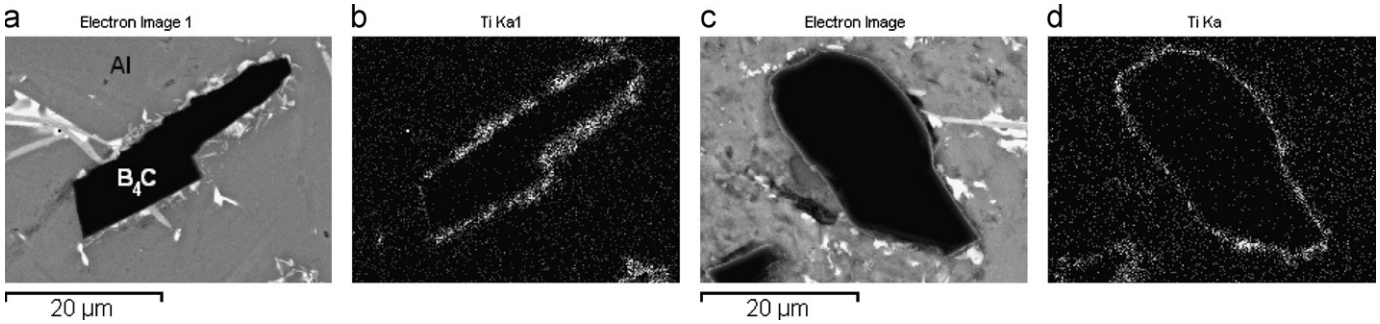


Fig. 2. (a) and (c) BSI SEM images and (b) and (d) matching Ti elemental maps of 15% and 19% reinforced composites respectively.

Table 4
Physical properties and hardness values.

Specimen	Nominal volume fraction (%)	Experimental volume fraction (%)	Particle addition yield (%)	Theoretical density (g/cm^3)	Experimental density (g/cm^3)	%Porosity	Hardness (HV)
AlSi9Cu3Mg–15% B_4C	16.20	14.83 ± 2.70	91.54	2.75	2.74 ± 0.0108	0.33	119.03 ± 2.68
AlSi9Cu3Mg–19% B_4C	21.50	18.71 ± 5.15	87.02	2.77	2.74 ± 0.0098	1.12	135.15 ± 5.35

Table 5
Experimental plan with results.

Std. order	Run order	Factor 1	Factor 2	Factor 3	Factor 4	Avg. COF	Wear rate (mg/m)	Wear rate of pins (mg/m)
		A: volume fraction (%)	B: velocity (m/s)	C: load (N)	D: distance (m)			
2	1	19	0.02	20	200	0.81 ± 0.10	0.01950	0.0015
9	2	15	0.02	20	400	0.81 ± 0.12	0.02075	0.0033
12	3	19	0.03	20	400	0.86 ± 0.11	0.02350	0.0060
7	4	15	0.03	40	200	0.53 ± 0.04	0.02150	0.0050
8	5	19	0.03	40	200	0.70 ± 0.08	0.02300	0.0095
14	6	19	0.02	40	400	0.80 ± 0.08	0.03650	0.0365
16	7	19	0.03	40	400	0.70 ± 0.06	0.01750	0.0035
11	8	15	0.03	20	400	0.79 ± 0.11	0.01400	0.0033
1	9	15	0.02	20	200	0.74 ± 0.10	0.00650	0.0050
13	10	15	0.02	40	400	0.74 ± 0.08	0.03100	0.0310
3	11	15	0.03	20	200	0.57 ± 0.06	0.02000	0.0080
5	12	15	0.02	40	200	0.48 ± 0.03	0.02450	0.0060
6	13	19	0.02	40	200	0.85 ± 0.08	0.04450	0.0140
4	14	19	0.03	20	200	0.81 ± 0.12	0.02350	0.0040
10	15	19	0.02	20	400	0.98 ± 0.15	0.03125	0.0043
15	16	15	0.03	40	400	0.51 ± 0.04	0.02125	0.0070

composites [26] and Canakci and Arslan detected approximately 3% porosity in stir-cast AA2024-10 vol% composites [19].

3.2. Dry sliding wear behaviour

Table 5 provides the experimental plan and the experimental results for average COF values and wear rate values both in composite specimens and counter materials.

3.2.1. Analysis of coefficient of friction values

COF graphs for light wear conditions (run orders 9 and 1 in Table 3 for 15% and 19% reinforced composites, respectively) and harsh wear conditions (run orders 16 and 7 in Table 3 for 15% and 19% reinforced composites, respectively) are given in Fig. 3. Similar trends were observed for the other conditions but with different average COF values. The average COF values are in the range of 0.48 and 0.98. In all conditions, COF values of 19% B_4C reinforced composites were higher than 15% B_4C reinforced composites. Furthermore, COF values are almost linearly increased during sliding distance.

The COF values were statistically investigated using the Minitab 15 statistical software. Fig. 4(a) shows the normal probability plot for average COF values. As can be seen on the graph, average COF values are reasonably fitted to normal distribution. Fig. 4(b) shows the main effect plots for average COF values. Average COF values are increased with volume fraction and sliding distance and decreased with sliding velocity and normal load.

Table 6 shows the results of the analysis of variance (ANOVA) table with the average COF values. ANOVA table shows source, degree of freedom (DF), sum of squares (SS), mean squares (MS), F value and percentage of contribution (P%). In the present work, only double interactions are investigated for all responses and level of confidence is chosen as 95%. The last column of the table shows the percentage of contribution, P (%), of each factor on the total variation indicating the degree of influence on the result. Percentage of contribution is calculated using the following formula [57,58]:

$$P\,(\%) = \frac{SS_F}{SS_T} \times 100 \tag{3}$$

where SS_F is the sum of squares of the factors or the interactions and SS_T is total sum of squares. The factors and the interactions

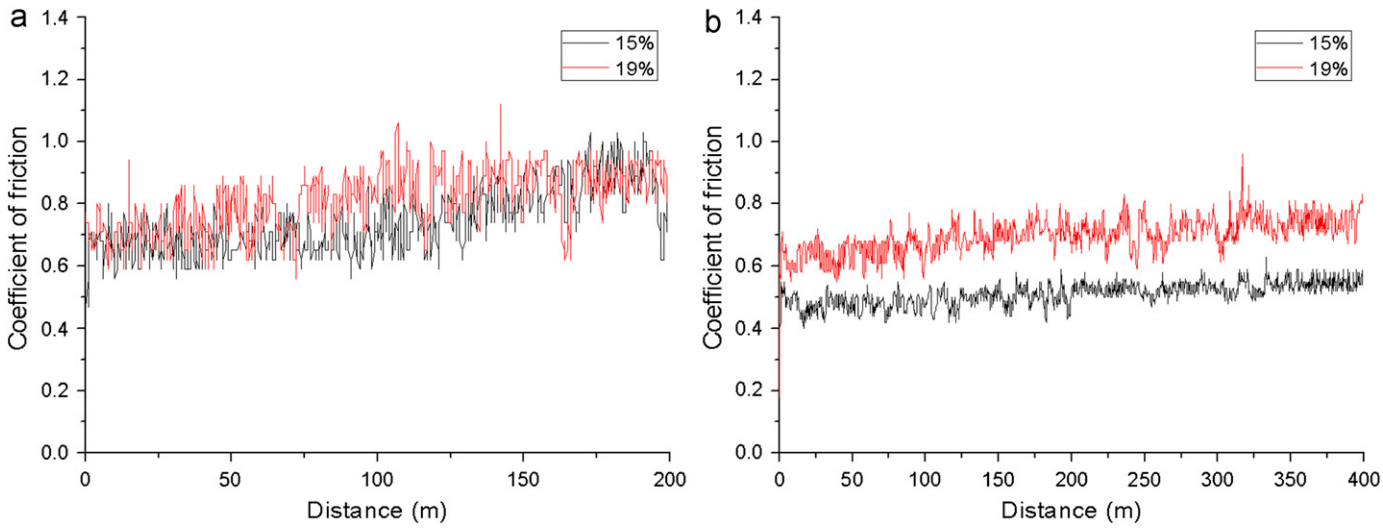


Fig. 3. COF graphs for (a) light and (b) harsh wear conditions.

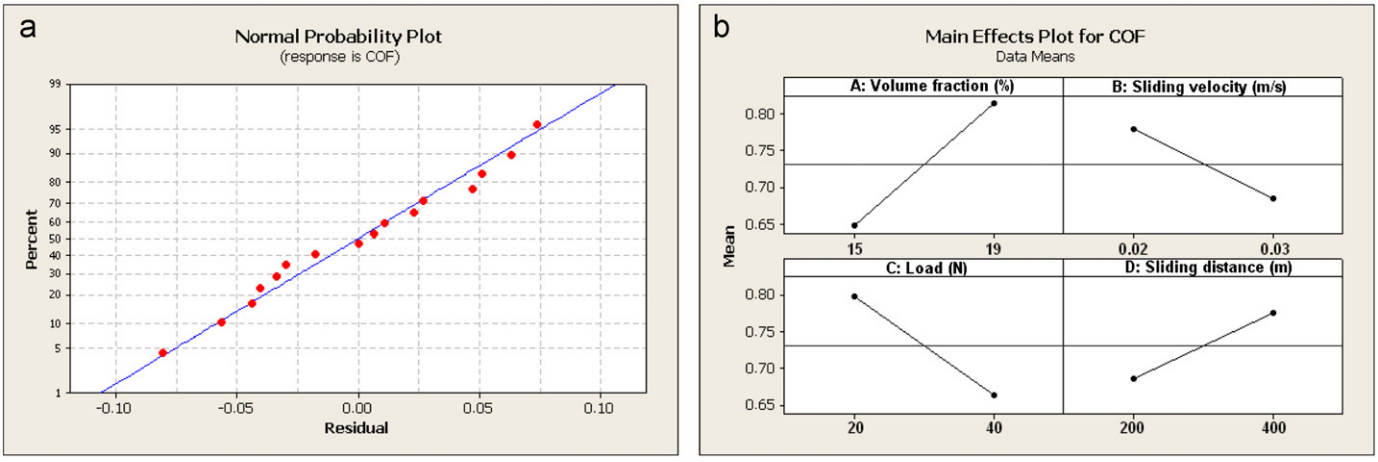


Fig. 4. (a) Normal probability and (b) main effect plots for average COF.

Table 6
ANOVA table for average COF.

Source[a]	DF	SS	MS	*F*	*P* (%)
A	1	0.1110110	0.1110110	17.79	36.41
B	1	0.0361430	0.0361430	5.79	11.86
C	1	0.0725760	0.0725760	11.63	23.81
D	1	0.0324050	0.0324050	5.19	10.63
A*B	1	0.0000050	0.0000050	0.00	0.00
A*C	1	0.0037830	0.0037830	0.61	1.24
A*D	1	0.0078090	0.0078090	1.25	2.56
B*C	1	0.0009330	0.0009330	0.15	0.31
B*D	1	0.0022490	0.0022490	0.36	0.74
C*D	1	0.0067420	0.0067420	1.08	2.21
Error	5	0.0311950	0.0062390		10.23
Total	15	0.3048520			100

[a] A: volume fraction (%); B: sliding velocity (m/s); C: load (N); D: sliding distance (m).

that have bigger *F* value than $F_{\alpha=5\%}$ and bigger *P* (%) value than the *P* (%) value of the error associated are taken as statistically and physically significant factors and interactions [57].

Analysis of the ANOVA table for average COF values (Table 6) showed that volume fraction ($P=36.41\%$) presented the strongest statistical and physical significance on the average COF values, followed by load ($P=23.81\%$). Other factors and interactions do not present statistical significance on the average COF values within the confidence level chosen.

In the literature, testing conditions for dry sliding of Al–B_4C composites are not similar with the present work. Particularly, for reciprocal sliding of Al–B_4C composites, contact pressures are much higher than the present study and the type and/or geometry of the counter material is different. In the present work, contact pressures are 1.02 and 2.04 MPa for 20 N and 40 N normal loads, respectively. Meydanoglu et al. studied reciprocal dry sliding of hot pressed Al–B_4C (10 wt%) composites against Al_2O_3 ball with 10 mm diameter with 100 g load, 0.02 and 0.09 m/s sliding velocity and 120 m sliding distance. The authors obtained different COF values with average particle size and sliding velocity. For 10 μm B_4C reinforced composites, average COF values are 0.93 ± 0.04 and 0.69 ± 0.11 and for 25 μm B_4C reinforced composites, the values are 1.10 ± 0.04 and 0.89 ± 0.13 against 0.02 and 0.09 m/s sliding velocity, respectively [41]. Hemanth studied unidirectional (pin-on-disc) dry sliding wear of Al–12% Si matrix B_4C_p reinforced (3–12 vol% insteps of 3 vol%) composites produced by vortex. The author used oil quenched SCM 4 (equivalent to AISI 4140) counter material, three different loads (10, 20 and 30 N), six sliding speeds (0.3–1.8 insteps of 0.3 m/s) and constant sliding distance (3000 m). As a comparison

with the present study; the author measured 0.7 COF value for 12% reinforced composite under 0.03 m/s sliding velocity and 30 N normal load [20]. In the present study, with 15% particle volume fraction, 0.03 m/s sliding velocity and 20 N normal load (corresponds to similar contact pressure), 0.57 and 0.79 average COF values were measured for 200 and 400 m sliding distances, respectively.

3.2.2. Analysis of wear rate values of specimens

Normal probability plot of wear rate values of specimens is shown in Fig. 5(a). As can be seen on the graph, the values are reasonably fitted to normal distribution. Fig. 5(b) shows the main effect plots for wear rate values. Wear rate values increased with volume fraction, load and sliding distance and decreased with sliding velocity.

Analysis of the ANOVA table for the wear rate values (Table 7) showed that load (P=19.43%) presented the strongest statistical and physical significance on the wear rate values, followed by volume fraction (P=18.79%). B*C interaction (sliding velocity*load) also presented statistical and physical significance on the wear rate values (P=16.66%). Other factors and interactions do not present statistical significance on the wear rate values within the confidence level chosen.

It is generally accepted that during the dry sliding of AMCs, as normal load increases the wear rate also increases. It is also expected that if particle volume fraction increases the wear rate decreases. However, statistical analysis showed that there is an increase in the wear rate values with the increment in the volume fraction.

As given in Table 4, the porosity values of AlSi9Cu3Mg-19% B_4C composite is higher than AlSi9Cu3Mg–15% B_4C. Besides, hardness of the 19% reinforced composite is not as higher as expected than the 15% reinforced composite. It was concluded that this small difference in the hardness value is mainly due to the higher porosity of the 19% reinforced composite. Furthermore, due to the higher porosity, the subsurface cracks may connect easier in 19% reinforced composites as compared to the 15% composites. Hence, the amount of removing particles can be expected more in the 19% reinforced composites than the 15% composites. Therefore, due to the third body effect of those particles, the wear rate of the 19% reinforced composite is higher than the 15% reinforced composite. However, it is concluded that the third body effect is not dominant on the wear mechanism. It is observed from the microstructures that the huge amounts of the reinforcing particles are still intact on the surface after sliding. It should be underlined that, due to the extremely higher hardness of the B_4C particles, under dominant third body effect conditions, the increment in the wear rate values can be expected to increase dramatically which did not observed in the present system.

3.2.3. Analysis of wear rate values of counter materials

Normal probability plot of wear rate values in counter material is given in Fig. 6(a). As can be seen on the graph, the values are reasonably fitted to normal distribution. Fig. 6(b) shows the main effect plots for wear rate by weight loss values in counter material. Wear rate values increased with volume fraction, load and sliding distance and decreased with sliding velocity. The main effects of factors generally showed the same tendency with wear rate values in samples but with different percentages.

Analysis of the ANOVA table for the wear rate values in counter materials (Table 8) showed that load (P=24.54%) presented the strongest statistical and physical significance on the wear rate values, followed by B*C (sliding velocity*load) interaction (P=20.01%). Other factors and interactions do not present statistical significance on the wear rate values in counter material within the confidence level chosen.

When the wear rate values in composite specimens and counter materials are compared, it can be seen that load is the most significant factor and B*C (sliding velocity*load) is the most significant interaction in both cases with different percentages of contributions. However, while volume fraction factor is statistically significant on the wear rate of composite specimens, it does not present statistical significance on the wear rate values in counter materials.

Table 7
ANOVA table for wear rate.

Source[a]	DF	SS	MS	F	P (%)
A	1	0.0002231	0.0002231	9.28	18.79
B	1	0.0001578	0.0001578	6.56	13.29
C	1	0.0002307	0.0002307	9.59	19.43
D	1	0.0000102	0.0000102	0.42	0.86
A*B	1	0.0000914	0.0000914	3.80	7.70
A*C	1	0.0000110	0.0000110	0.46	0.93
A*D	1	0.0000165	0.0000165	0.69	1.39
B*C	1	0.0001978	0.0001978	8.22	16.66
B*D	1	0.0000821	0.0000821	3.42	6.92
C*D	1	0.0000464	0.0000464	1.93	3.91
Error	5	0.0001202	0.0000240		10.12
Total	15	0.0011872			100

[a] A: volume fraction (%); B: sliding velocity (m/s); C: load (N); D: sliding distance (m).

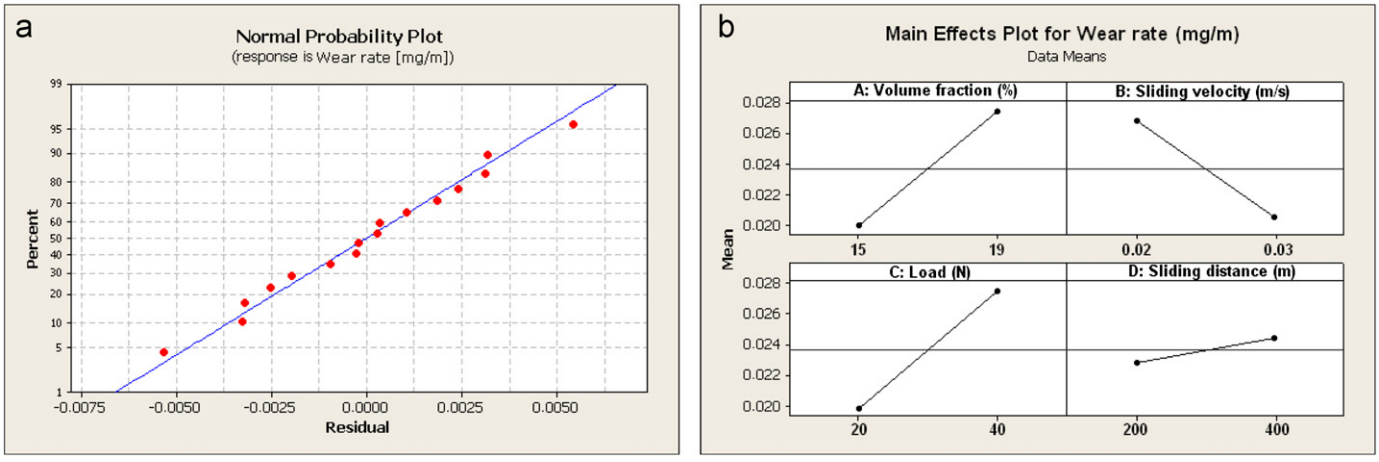


Fig. 5. (a) Normal probability and (b) main effect plots for wear rate.

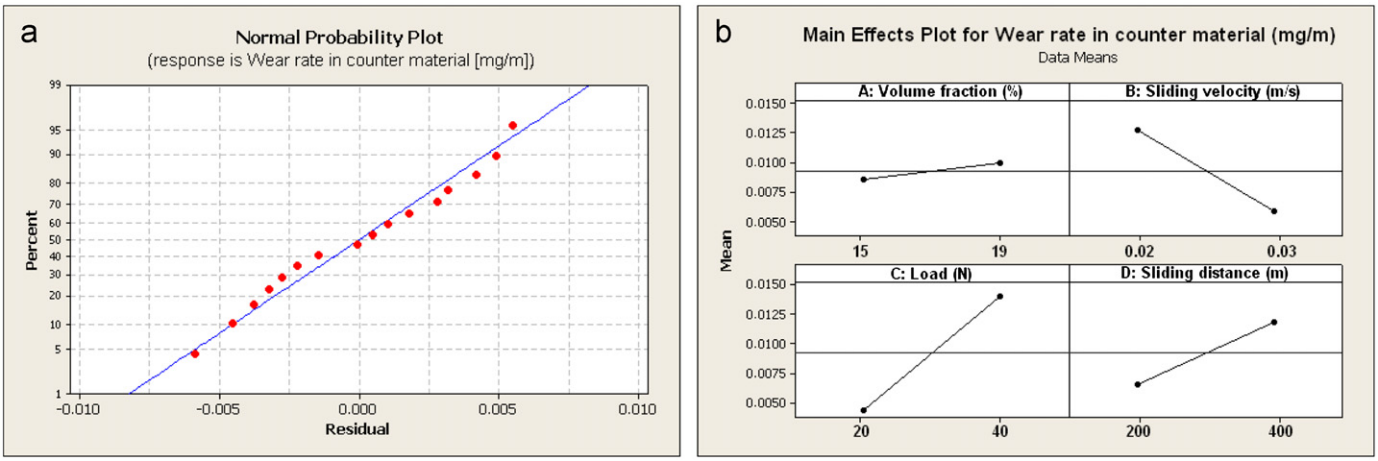


Fig. 6. (a) Normal probability and (b) main effect plots for wear rate in counter material.

Table 8
ANOVA table for wear rate values in counter material.

Source[a]	DF	SS	MS	*F*	*P* (%)
A	1	0.0000072	0.0000072	0.19	0.47
B	1	0.0001908	0.0001908	5.07	12.55
C	1	0.0003730	0.0003730	9.90	24.54
D	1	0.0001089	0.0001089	2.89	7.17
A*B	1	0.0000079	0.0000079	0.21	0.52
A*C	1	0.0000208	0.0000208	0.55	1.37
A*D	1	0.0000000	0.0000000	0.00	0.00
B*C	1	0.0003041	0.0003041	8.07	20.01
B*D	1	0.0001908	0.0001908	5.07	12.55
C*D	1	0.0001280	0.0001280	3.40	8.42
Error	5	0.0001883	0.0000377		12.39
Total	15	0.0015198			100

[a] A: volume fraction (%); B: sliding velocity (m/s); C: load (N); D: sliding distance (m).

3.2.4. *Microstructural analysis of the worn surfaces*

Microstructure of the worn surfaces of composite specimens and matching counter materials' surfaces is investigated using OM and SEM for light and harsh wear conditions. The morphology of the worn surface of composite specimens is shown in low magnification SEM images in Fig. 7. Parallel sliding marks along the sliding direction are visible on the worn surfaces for both volume fraction and both conditions. However, 19% reinforced composites have relatively smooth surface for both conditions. Matching EDS analysis results are also given in Fig. 7. As can be seen on the EDS spectra, the presence of Fe and O is detected for all conditions which prove that there is a material transfer from counter material and that transferred material probably is oxidised during the sliding.

In higher magnification examinations, the worn surfaces showed the following features: (i) grooves, (ii) protrusions, (iii) craters, (iv) flakes, (v) iron on worn surface, (vi) oxide on worn surface, (vii) plastic deformation, (viii) cracks, and (ix) heap of loose debris. While grooves and Fe and O on the worn surfaces are common in both volume fractions and conditions, other features are observed in some conditions.

Fig. 8 shows the B_4C protrusions on the worn surface of 15% B_4C reinforced composite worn in light conditions. Those protrusions was only observed in light conditions. In harsh conditions, they probably get flat or covered with wear debris.

Fig. 9 shows the craters on the worn surface of 19% B_4C reinforced composite worn in harsh conditions. It has been reported that detached layer in the form of craters or cavities indicates locally adhesive wear due to the formation of and breaking of microwelds during sliding [24].

Fig. 10 shows SEM image of a large flaky piece which is about to be dislodged from the surface. The EDS analysis taken from the marked area in Fig. 10(a) shows that the flake contains Al, Fe (from counter material) and oxides (Fig. 10(b)).

It has been reported that, for microstructures containing hard second-phase particles, if sufficient plastic deformation occurred during sliding wear, crack nucleation was favoured at these particles. In this case, inter-particle spacing is an important variable and crack propagation controlled the wear rate. Void formation was primarily attributed to the plastic flow of the matrix metal around these hard second-phase particles. Void formation occurred very readily around the particles but crack propagation occurred very slowly. The depth at which the void nucleation was initiated and the void size tended to increase with increased COF and applied load [59]. Plastic deformation and cracks related to delamination wear were observed on worn surfaces. However, delamination wear is not the dominant wear mechanism in all cases that studied. Fig. 11(a) shows the plastic deformation traces and Fig. 11(b) shows the cracks on the worn surfaces.

Fig. 12 shows SEM image of uncompacted powdery debris contains Al, Fe and oxides that confirmed with the EDS analysis taken from the same area. It has been reported that the loose wear debris has the same structure and composition as the transferred layer [59]. Therefore, together with COF values it has concluded that a tribolayer containing Fe, Al and oxides formed during the sliding on the surfaces of composite specimens. Same features (large flaky piece and uncompacted powdery debris) were observed by Shorowordi et al. worked with the unidirectional dry sliding of Al–13%B_4C_p composites against a commercial phenolic brake pad [22].

Surfaces of pins (counter material) were also investigated with SEM and EDS. Low magnification SEM images are given in Fig. 13. It is visible on the images that pins have parallel sliding marks along the sliding direction on the worn surfaces for both volume fraction and both conditions. However, grooves are shallower compared to composite worn surfaces. In addition to grooves, some dark regions and patches can be seen on the worn surfaces of pins. Since the images are taken on BSI mode, these regions appear to contain Al or oxides. Matching EDS analysis results taken from the images are also given in Fig. 13 confirm that worn surfaces of pins contains relatively high amounts of Al and O. Furthermore, analysis also contains C in pins worn again 15% B_4C reinforced composites and both B and C in pins worn against 19% B_4C reinforced composites

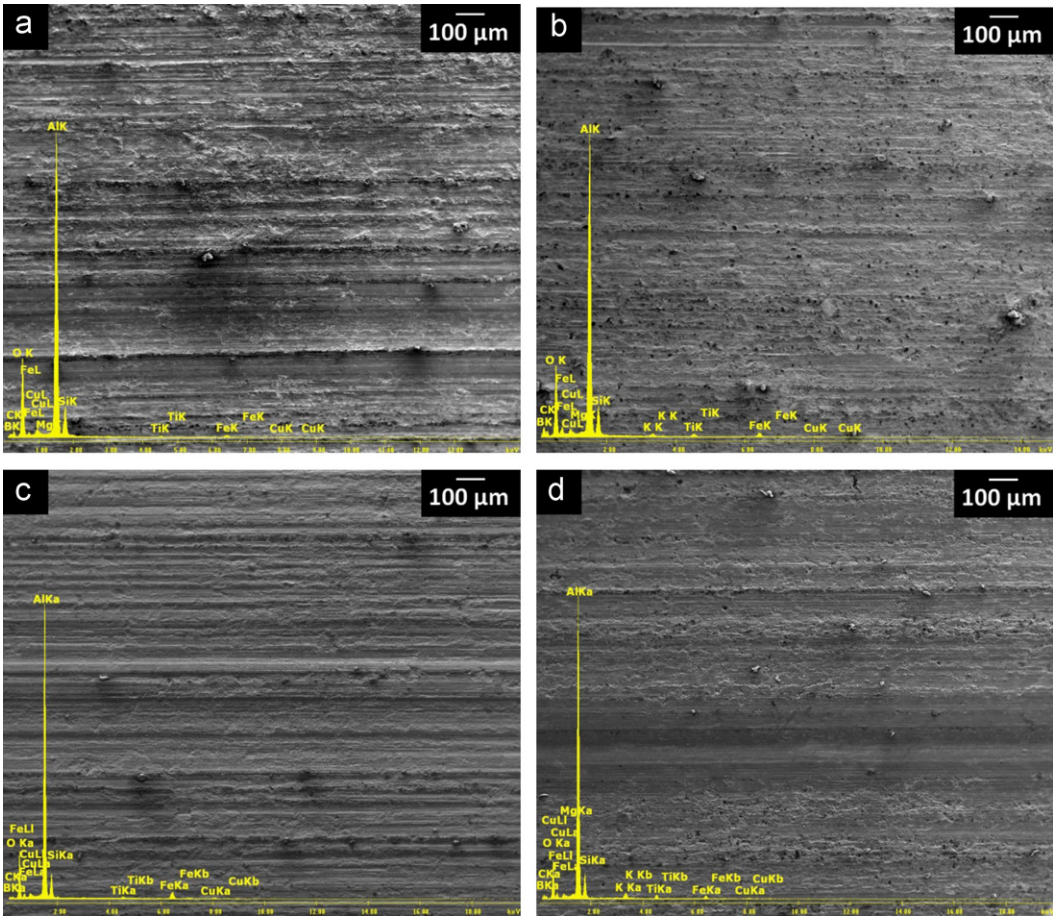


Fig. 7. Low magnification secondary electron (SE) SEM images of the worn surfaces and matching EDS analysis for (a) 15%, (b) 19% reinforced composites worn in light conditions and (c) 15%, (d) 19% reinforced composites worn in harsh conditions.

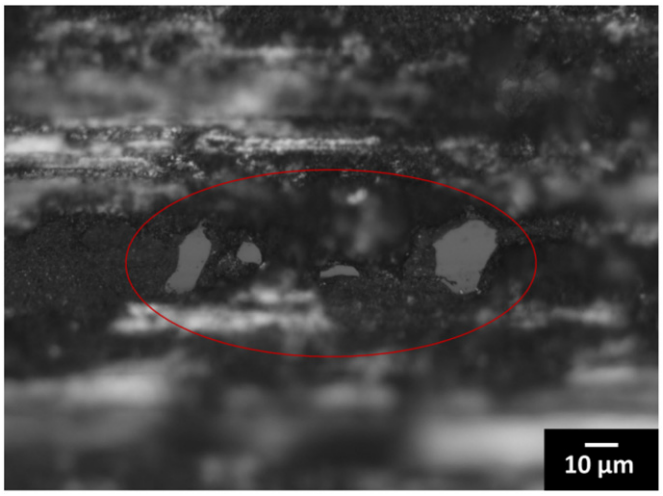


Fig. 8. OM image showing B_4C protrusions on the worn surface of 15% reinforced composite worn in light conditions.

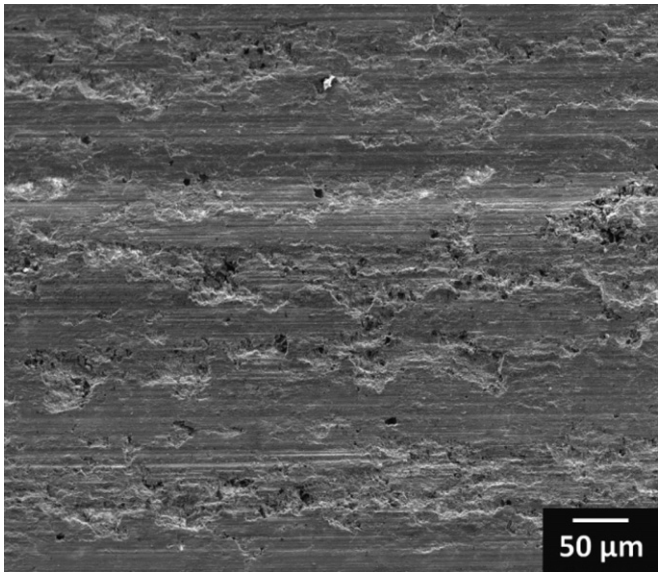


Fig. 9. SE SEM image of the craters on the worn surface of 19% B_4C reinforced composite worn in harsh conditions.

means that there is also reinforcing material transfer from composite materials to pins during the sliding.

In higher magnification examinations in pins, the worn surfaces showed the following features: (i) craters, (ii) patches and (iii) adhered flakes. Fig. 14 shows the craters on the surface of the pin worn against 19% B_4C reinforced composite in light conditions. Those craters also confirms adhesive wear due to the formation of and breaking of microwelds during sliding, similar to the composite worn surfaces that are given in Fig. 9.

Fig. 15(a) shows an adhered flake on the on the surface of the pin worn against 15% B_4C reinforced composite in harsh

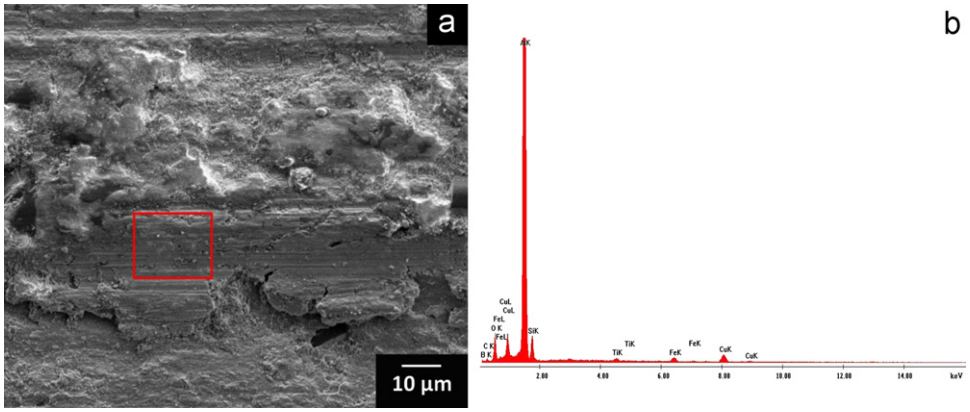


Fig. 10. (a) SE SEM images of a large flaky piece is about to be dislodged from the surface from 15% B_4C reinforced composite worn in light conditions and (b) EDS analysis taken from the marked area.

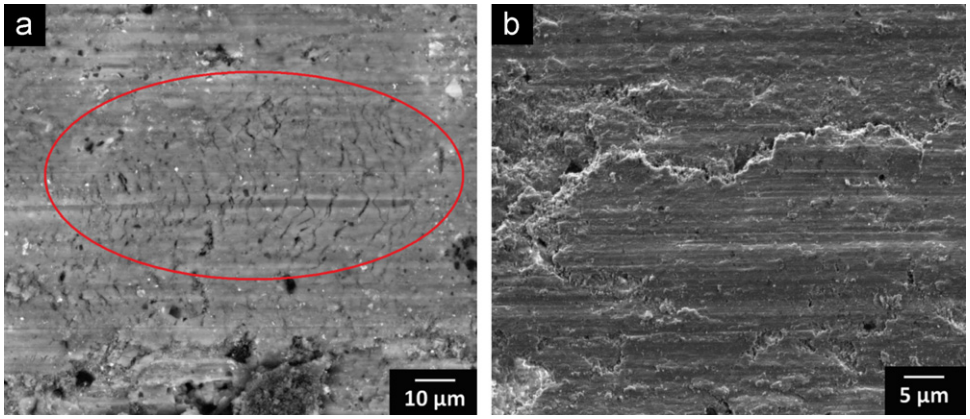


Fig. 11. Plastic deformation on (a) 15% reinforced composite worn in light conditions and (b) cracks on 19% reinforced composite worn in harsh conditions in BSI and SE SEM images, respectively.

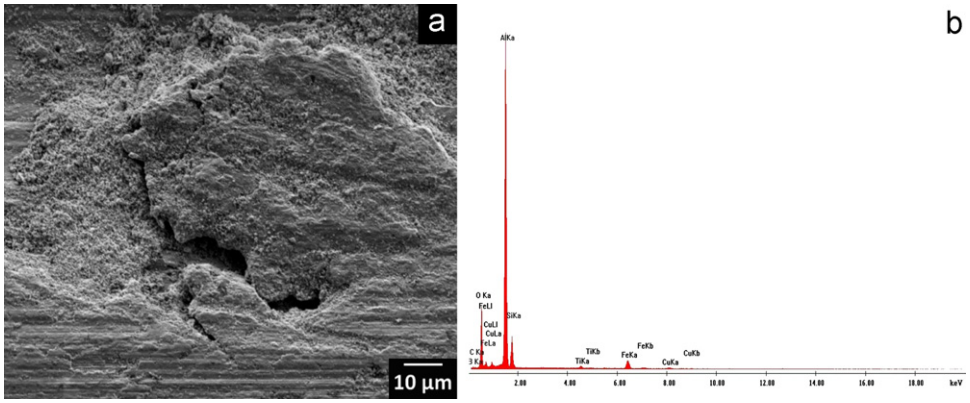


Fig. 12. (a) SE SEM image and (b) matching EDS analysis of uncompacted powdery debris from 19% B_4C reinforced composite worn in harsh conditions.

conditions. After the EDS analysis taken from those flake (Fig. 15b) it has deduced that this flake detached from the composite sample due to the delamination wear and adhered to the pins surface during the sliding.

Fig. 16(a) shows the loose and compacted oxidised patches on the surface of the pin worn against 19% B_4C reinforced composite in harsh conditions. EDS analysis taken from the loose and compacted areas are given in Fig. 16(b) and (c) respectively. It has concluded from the EDS analysis that the patches have the similar composition with the tribolayer.

3.2.5. Wear mechanism

Due to COF graphs and characterisation of wear surfaces, the wear mechanism has been suggested as following: At the initial stage, load is mainly borne by reinforcing particles and it results with relatively lower COF values. As sliding time increases, B_4C particles abrade the counter material. When grooves occurred on the counter materials surface, counter materials surface starts to contact with the aluminium matrix surface. This contact results with the adhesive wear which can be distinguished by craters and adhered flakes in both surfaces and abrasive wear which can be

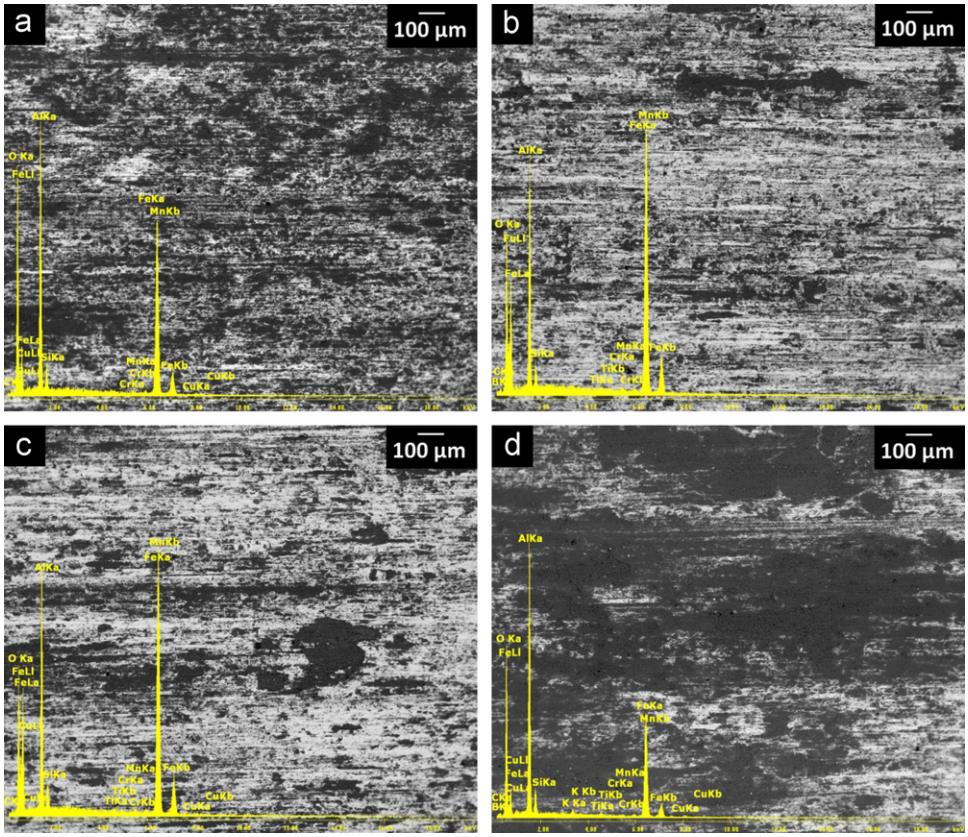


Fig. 13. Low magnification BSI SEM images of the worn surfaces and matching EDS analysis of pins worn against (a) 15%, (b) 19% reinforced composites in light conditions and (c) 15%, (d) 19% reinforced composites in harsh conditions.

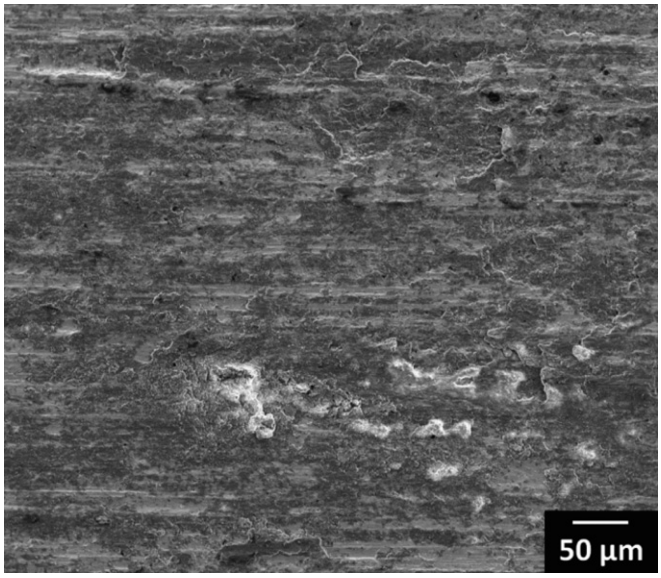


Fig. 14. Craters on SE SEM image of the surface of the pin worn against 19% B_4C reinforced composite in light conditions.

distinguished by grooves in composite surfaces. Another result of this contact is the forming of mechanically mixed layer which can be detected by elements of counter wear pair and oxides on the wear surfaces. Therefore, while the contact is mainly metal–ceramic at the initial stage, as sliding time increases, the metallic character of the contacting wear surface increases. This situation leads to increasing of COF values during the sliding. On the other hand, due to plastic deformation, cracks start to nucleate and propagate which causes delamination wear. Therefore, wear mechanism can be suggested as a combination of adhesive, abrasive, and delamination wear.

4. Conclusions

AlSi9Cu3Mg alloy matrix composites reinforced with 15 and 19 vol% B_4C_p were produced by squeeze casting route at 850 °C under low vacuum with the addition of titanium-containing flux. The samples were subjected to reciprocating wear tests against AISI 4140 pin under dry sliding conditions. The effects of B_4C volume fraction, sliding velocity, applied load and sliding distance on reciprocal dry wear behaviour of composites were studied using general full factorial experimental design. From data analysis and microstructural investigations, the followings can be concluded:

- Due to the proper production route with K_2TiF_6 addition, relatively homogenous particle distribution, relatively high volume fraction and relatively decreased porosity values were obtained.
- From analysing the experimental analysis, it can be concluded that
  - COF and wear rates increased as volume fraction increased;
  - COF and wear rates decreased as velocity increased;
  - COF decreased and wear rates increased as load increased; and
  - COF and wear rates increased as distance increased.
- From data analysis, it can be concluded that volume fraction is the most important factor for COF, while load is the most important factor for wear rates.

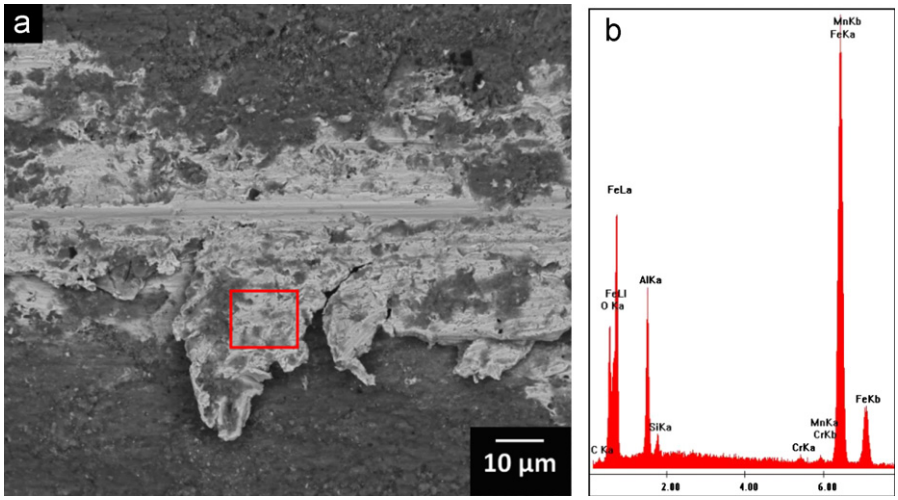


Fig. 15. (a) Adhered flake on BSI SEM image of the surface of the pin worn against 15% B_4C reinforced composite in harsh conditions and (b) EDS analysis taken from the marked area.

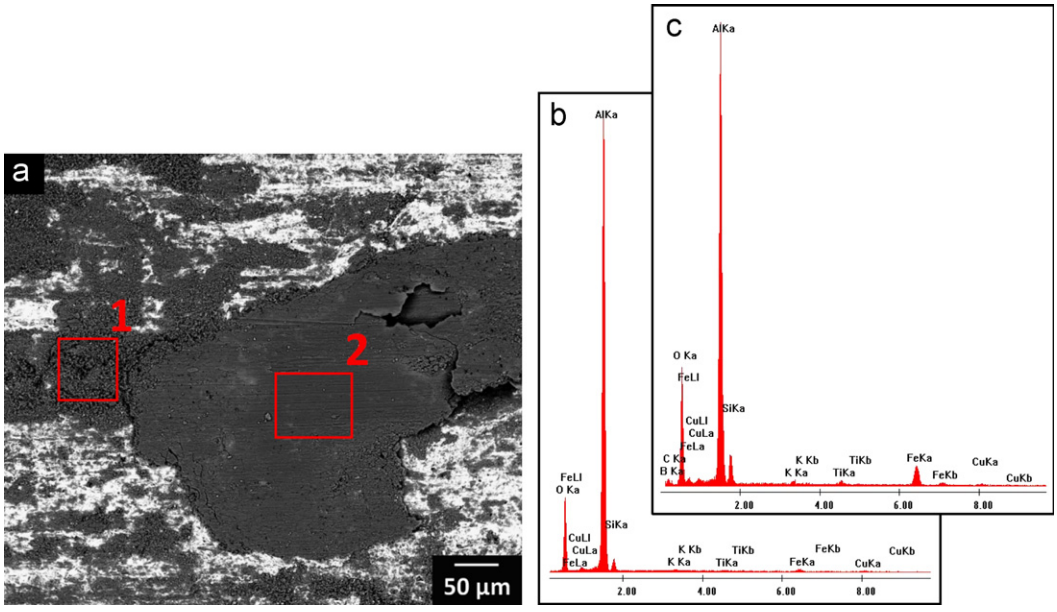


Fig. 16. (a) Oxide patches on BSI SEM image of the surface of the pin worn against 19% B_4C reinforced composite in harsh conditions and (b) and (c) EDS analysis taken from "1" and "2" areas indicated in "a".

- Wear mechanism can be suggested as a combination of adhesive, abrasive, and delamination wear.

Acknowledgements

This study was partially supported by TUBITAK (The Scientific and Technological Research Council of Turkey) under Grant No. 107M338. The authors would also like to thank for their kind help to Prof. Ö. Keleş from Istanbul Technical University for experimental design studies, and Prof. J. Gomes and Mr. S. Carvalho from University of Minho for tribological studies.

References

[1] K. Tokaji, Fatigue and Fracture of Engineering Materials and Structures 28 (2005) 539–545.
[2] K.B. Lee, et al., Metallurgical and Materials Transactions A—Physical Metallurgy and Materials Science 32A (4) (2001) 1007–1018.
[3] I. Kerti, F. Toptan, Materials Letters 62 (2008) 1215–1218.
[4] R. Ipek, Journal of Materials Processing Technology 162–163 (2005) 71–75.
[5] F. Bedir, Materials & Design 28 (2007) 1238–1244.
[6] A. Kalkanlı, S. Yılmaz, Materials & Design 29 (2008) 775–780.
[7] I. Kerti, Materials Letters 59 (2005) 3795–3800.
[8] K.B. Khan, et al., Materials Science and Engineering: A 427 (2006) 76–82.
[9] H. Zhang, et al., Materials Science and Engineering: A 384 (2004) 26–34.
[10] M. Aizenshtein, et al., Scripta Materialia 53 (2005) 1231–1235.
[11] J. Jung, S. Kang, Journal of the American Ceramic Society 87 (1) (2004) 47–54.
[12] X. Zhu, et al., Surface and Coatings Technology 202 (2008) 2927–2934.
[13] N.K. Shrestha, et al., Surface and Coatings Technology 200 (2005) 2414–2419.
[14] C.A. Smith, Discontinuous reinforcements for metal-matrix composites, ASM Handbook: vol. 21, Composites, ASM International, 2001.
[15] Z. Zhang, et al., Journal of Materials Science 42 (2007) 7354–7362.
[16] K.M. Shorowordi, et al., Journal of Materials Processing Technology 142 (2003) 738–743.
[17] F. Toptan, et al., Materials Science Forum 636–637 (2010) 192–197.
[18] F. Toptan, et al., Materials & Design 31 (2010) S87–S91.
[19] A. Canakci, F. Arslan, Proceedings of the 11th International Materials Symposium, Denizli, 2006, pp. 382–389.
[20] J. Hemanth, Wear 258 (2005) 1732–1744.
[21] A. Canakci, F. Arslan, Proceedings of 12th International Metallurgical Materials Congress, Istanbul, 2005, pp. 772–783.
[22] K.M. Shorowordi, et al., Wear 261 (2006) 634–641.

[23] K.M. Shorowordi, et al., Wear 256 (2004) 1176–1181.
[24] H.R. Lashgari, et al., Materials & Design 31 (2010) 2187–2195.
[25] H.R. Lashgari, et al., Materials & Design 31 (2010) 4414–4422.
[26] A. Mazahery, M.O. Shabani, Journal of Materials Engineering and Performance 21 (2011) 247–252.
[27] A. Canakci, Journal of Materials Science 46 (2011) 2805–2813.
[28] A.R. Kennedy, B. Brampton, Scripta Materialia 44 (2001) 1077–1082.
[29] D.C. Halverson, et al., Journal of the American Ceramic Society 72 (5) (1989) 775–780.
[30] A.R. Kennedy, A.E. Karantzalis, Materials Science and Engineering: A 264 (1999) 122–129.
[31] D.C. Halverson, et al., US Patent No. 4,605,440, 1986.
[32] A.R. Kennedy, Journal of Materials Science 37 (2002) 317–323.
[33] J. Hashim, et al., Journal of Materials Processing Technology 92–93 (1999) 1–7.
[34] H. Sevik, S.C. Kurnaz, Materials & Design 27 (2006) 676–683.
[35] K. Laden, et al., Tribology Letters 8 (2000) 237–247.
[36] Sur, et al., Journal of the Faculty of Engineering and Architecture of Gazi University 20 (2) (2005) 233–238.
[37] M. Kök, Fen ve Mühendislik Dergisi 4 (2001) 131–142.
[38] S. Buytoz, H. Eren, Fırat University, Journal of Science and Engineering 19 (2) (2007) 209–216.
[39] M.R. Rosenberger, et al., Wear 259 (2005) 590–601.
[40] F. Tang, et al., Wear 264 (2008) 555–561.
[41] O. Meydanoglu, et al., Proceedings of the 11th International Materials Symposium, Denizli, 2006, pp. 270–272.
[42] H. Mindivan, Materials Letters 64 (2010) 405–407.
[43] G. Akin, et al., Proceedings of 12th International Metallurgical Materials Congress, Istanbul, 2005, pp. 735–740.
[44] V.R. Rajeev, et al., Tribology International 43 (2010) 1532–1541.
[45] S. Anoop, et al., Materials & Design 30 (2009) 3831–3838.
[46] S. Suresha, B.K. Sridhara, Materials & Design 31 (2010) 1804–1812.
[47] S. Suresha, B.K. Sridhara, Composites Science and Technology 70 (2010) 1652–1659.
[48] S. Suresha, B.K. Sridhara, Materials & Design 34 (2012) 576–583.
[49] J.S.S. Babu, et al., Materials & Design 32 (2011) 3920–3925.
[50] S. Kumar, V. Balasubramanian, Tribology International 43 (2010) 414–422.
[51] S. Basavarajappa, et al., Materials & Design 28 (2007) 1393–1398.
[52] Y. Şahin, Tribology International 43 (2010) 939–943.
[53] S. Basavarajappa, G. Chandramohan, Journal of Materials Science and Technology 21 (2005) 845–850.
[54] Y. Sahin, Materials & Design 24 (2003) 95–103.
[55] S. Naher, et al., Journal of Materials Processing Technology 166 (2005) 430–439.
[56] P. Shen, et al., Materials Science and Engineering: A 454–455 (2007) 300–309.
[57] J.P. Davim, Journal of Materials Processing Technology 132 (2003) 340–344.
[58] N.A. Shuaib, et al., IJET–IJENS 11 (01) (2011) 182–187.
[59] R.L. Deuis, et al., Composites Science and Technology 57 (1997) 415–435.